International Journal of Multiphase Flow 42 (2012) 62–73

Contents lists available at SciVerse ScienceDirect

International Journal of Multiphase Flow

journal homepage: www.elsevier.com/locate/ijmulflow

Multiphase capillary flows

Federico Maggi *, Fernando Alonso-Marroquin

School of Civil Engineering, The University of Sydney, Bld. J05, Sydney 2006, NSW, Australia

ARTICLE INFO

Article history:
Received 5 November 2010
Received in revised form 17 January 2012
Accepted 24 January 2012
Available online 6 February 2012

Keywords:
Capillary flow
Multiphase flow
Lucas–Washburn equation
Water
Ethanol
Ether
Dodecane
Silicon
Air

ABSTRACT

We present here a model of the meniscus movement within uniform capillaries that explicitly accounts for the effect of the gas phase. The total momentum was assumed to change by the gravitational, viscous, surface, dissipative and boundary forces, and included dynamical effects due to variable contact angle and the reservoirs adjacent the capillary inlet and outlet. This two-phase equation was comprehensively tested against earlier models and records of two-phase systems (water, ethanol, dodecane, diethyl ether and silicon displacing air), capillary radii (0.1–4 mm), and under various gravitational accelerations ($g = 9.81$ m s^{-2} and $g \simeq 0.02$ m s^{-2}). The proposed framework predicted experimental capillary rise with higher correlation coefficient (98.84–99.98%) and smaller error (0.55–2.95%) as compared to earlier single-phase equations, which achieved lower correlations (72–99.99%) and larger errors ($\gg$1.1). Including the gas phase led to improvements up to about 6% depending on liquid characteristics. When also variable contact angle was included, the improvement increased by up to about 13% as compared to liquid-only phase and no variable contact angle. Dimensionless analyzes showed that gas-related effects were as important as inertia and reservoir effects. Supported by these results, we reject the hypothesis by which gas-related effects can be neglected in modeling capillary processes.

1. Introduction

The dynamics of liquids in capillaries has been under continuous attention within the classical fluid dynamics disciplines as well as in a variety of applied sciences such as groundwater and soil physics, plant physiology, medicine and, more recently, micro/nanotechnology and space applications (e.g., Ralston et al., 2008; Maggi and Pallud, 2010).

The first comprehensive treatment of the physics of capillary rise dates back to the works by Bell and Cameron (1906), Lucas (1918) and Washburn (1921), in which the basis for its understanding was presented in the form now commonly known as the Lucas–Washburn equation. For uniformly-circular capillaries and homogeneous non-compressible Newtonian liquids, Washburn described the meniscus movement assuming that it was only determined by the tension developing at the solid–liquid–gas interface, the gravitational and viscous forces acting on the liquid, and the boundary pressures, but excluded any effects of the gaseous phase and the inertial effects of the reservoirs at the capillary boundaries. The Lucas–Washburn (LW) equation was proven to be reliable in a wide variety of cases. However, because corrections to the initial conditions had to be taken to overcome a singularity point, it describes more properly the asymptotic flow regime. Regardless of this singularity, the accuracy of the LW equation decreases when it is used to describe liquids with decreasing density and dynamic viscosity (e.g., ethers *versus* water), for relatively high accelerations and velocities (e.g., at the onset of flow), for increasing capillary length, and in microgravity or supergravity conditions. In these cases, viscous effects in both liquid and gaseous phases, inertia, as well as other dissipative forces can substantially affect the meniscus velocity within the capillary.

There have been several improvements to the original LW framework, the most relevant of which to our work are briefly introduced. Blake and Haynes (1969) proposed an approach based on the Eyring's theory or rate processes (Eyring, 1935) to describe how the angle at the three-phase contact line changes when the meniscus is moving within the capillary. According to their approach, which is based on first principles conversely to other empirical frameworks, the contact angle changes as an hyperbolic function of the meniscus velocity. Although dynamic contact angle appears to be largely accepted after theoretical and experimental evidence in capillary processes (e.g., Joos et al., 1989; Hamraoui et al., 2000; Bico and Quere, 2001; Martic et al., 2002; Popescu et al., 2008; Hilpert, 2009) and in the wider context of wetting and non-wetting surfaces (e.g., De Gennes, 1985; Cox, 1998), an exact expression has not yet been found that finds the largest consensus. Hence, we will refer next to the Blakes and Haynes' model as the most general expression for the arguments discussed later.

Szekely et al. (1971) included inertial effects of the liquid phase entering the capillary from the reservoir. This approach was successful in removing the singularity of the velocity at the initial point, but introduced a physical inconsistency that was only later overcome by Dreyer et al. (1994) and Xiao et al. (2006). Under

* Corresponding author.
E-mail address: federico.maggi@sydney.edu.au (F. Maggi).

0301-9322/$ - see front matter © 2012 Published by Elsevier Ltd.
doi:10.1016/j.ijmultiphaseflow.2012.01.011

suitable hypotheses, Dreyer et al. (1994) showed that the boundary forces at the capillary entrance depend nonlinearly on the meniscus velocity and acceleration.

The hydrodynamics in the liquid phase near the meniscus were investigated in Levine et al. (1980) who, under the hypothesis of invariant meniscus shape (i.e., sector of a sphere), arrived to the conclusion that a localized dissipative force scales with the height of the three-phase contact line relative to the meniscus depression and with an additional length scale linked to surface irregularities. The latter two contributions were described as functions of the sphere sector, capillary radius, slip coefficient, and contact angle, respectively (see Eq. 3.14, Levine et al., 1980).

More recently, Zhmud et al. (2000) introduced a nonlinear turbulent drag force in the LW equation, which contributes to decrease the meniscus velocity. This approach introduced two empirical dimensional parameters that required calibration but, more important, left unresolved the singularity at the initial condition and introduced a discontinuity of the first and second order in the capillary dynamics.

Whereas empirical approaches have led to improvements in the description of dynamical effects due to localized dissipation sources, the effect of multiple phases has been left relatively aside. Recognizing that neither the liquid nor the gaseous phase alone governs the dynamics of flows in capillaries, suggests that the coupled effect of liquid–gas interactions should explicitly be taken into account in as mechanistic way as possible. Our aim, therefore, is to specifically resolve the dynamics of multiphase capillary flows by extending the original Lucas–Washburn equation to the momentum rate of change to the liquid and gaseous phases within the capillary and the adjacent reservoirs.

After presenting the mathematical derivation of the multiphase capillary flow equation, we compare in Section 3 its performance against earlier models and existing experimental data of various liquids displacing air in capillaries of various radii and under terrestrial and microgravity. Next, we discuss in Section 4 aspects that require further investigation.

2. Theory

2.1. Derivation of the governing equation

We consider a uniform circular capillary of radius R and length L in contact with a liquid reservoir at the bottom and a gaseous reservoir at the top, both indefinitely extended. We define the control volume (CV) to be the capillary in its full length and the control surface (CS) its open boundaries at the two capillary ends (Fig. 1a). We assume that the meniscus at the liquid–gas interface moves within the capillary under the action of the surface tension, gravitational, viscous, conservative, non-conservative, and boundary forces. To describe the meniscus dynamics within capillaries, we couple the Reynolds transport theorem applied to the momentum in the capillary and to the Bernoulli energy density in the reservoirs.

Applying the Reynolds transport theorem to the rate of change of the momentum $P(t)$ within the capillary leads to

$$\begin{aligned}\frac{\mathrm{d}P(t)}{\mathrm{d}t} &= \frac{\partial}{\partial t}\int_{CV}\rho\vec{v}\,\mathrm{d}V + \int_{CS}\rho\vec{v}\cdot\vec{v}\vec{n}\,\mathrm{d}A = \\ &= \frac{\mathrm{d}}{\mathrm{d}t}\left\{\pi R^2\left[\rho_l h(t) + \rho_g(L-h(t))\right]v(t)\right\} - \pi R^2\rho_l v(t)^2 \\ &+ \pi R^2\rho_g v(t)^2 = \\ &= \pi R^2\left\{\rho_l h(t) + \rho_g[L-h(t)]\right\}\frac{\mathrm{d}v(t)}{\mathrm{d}t} = (m_l+m_g)\frac{\mathrm{d}v(t)}{\mathrm{d}t}, \end{aligned} \quad (1)$$

where $h(t)$ and $v(t)$ are the meniscus position and velocity at time t, ρ_l and ρ_g are the liquid and gaseous densities, and m_l and m_g are the liquid and gaseous masses, respectively. Eq. (1) shows that $\mathrm{d}P(t)/\mathrm{d}t$ depends on the rate of change of momentum of the liquid and gaseous phases within the CV, each representing an inertial force (i.e., I_l and I_g respectively). In writing Eq. (1) for open capillary ends, we have assumed that gas compressibility is negligible, whereas under different circumstances such as in close-end capillaries, gas compressibility should be included. Similarly, if the pressure of the fluids within the CV is substantially different than outside the CV, gas compressibility should be taken into account.

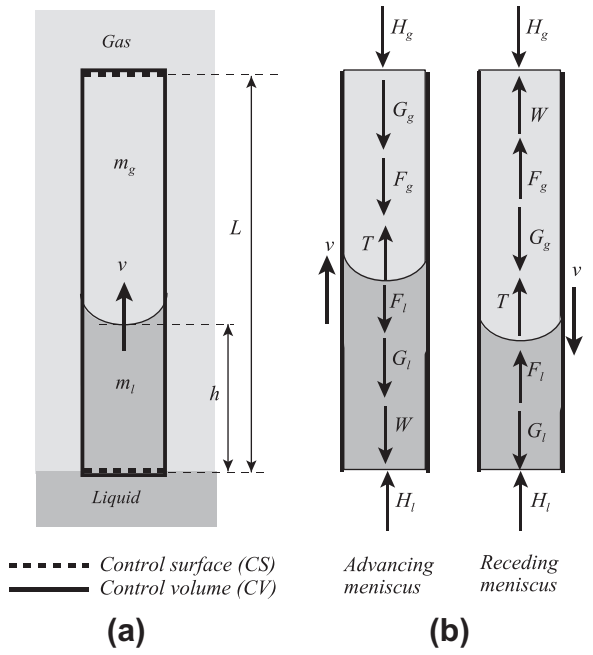

Fig. 1. (a) control volume (CV) and control surface (CS) of the fluids in a capillary of radius R and length L. (b) Forces acting within the capillary and at its boundaries.

According to the second Newton's law, $\mathrm{d}P(t)/\mathrm{d}t$ can be expressed as the resultant of all forces as (Fig. 1b)

$$T + \sum_{l,g}(G+F) + W + \Delta H = \frac{\mathrm{d}P(t)}{\mathrm{d}t}, \quad (2)$$

where T is the tension at the three-phase point of contact, the summation collects the gravitational and viscous forces G and F in the liquid and gaseous phases, respectively, W is a dissipative force located within an entrance length of the capillary occurring either in the gas or liquid phase depending on the flow direction, while ΔH is the force due to the pressure difference at two capillary ends (Fig. 1b).

The tension T is

$$T = 2\pi R\gamma\cos(\theta), \quad (3)$$

with γ the surface tension between the gaseous and liquid phases, and θ the contact angle between the liquid phase and the capillary wall. Various approaches have been proposed to describe θ as a function of v. Blake and Haynes (1969) used the Eyring's theory of rate processes to express the contact angle θ as the inverse sinhyperbolic function of v as

$$\cos(\theta) = \cos(\theta_\infty) - A\,\mathrm{arcsinh}\{Bv(t)\}, \quad (4)$$

where θ_∞ is the contact angle at rest. The parameters A and B are related to the molecular and thermodynamic properties of the solid–liquid–gas interfaces and are defined as (Blake and Haynes, 1969; Martic et al., 2002)

$$A = \frac{2nk_BT_K}{\gamma}, \quad B = \frac{1}{2K^0\lambda}, \tag{5}$$

with n the number of affected adsorption sites at the solid and liquid interfaces per unit area of solid interface, k_B the Boltzmann constant, T_K the temperature in kelvin, λ the average distance between adsorption sites, and K^0 the rate constant describing the frequency of molecular displacements at the three-phase contact line. Other approaches made use of similar nonlinear functions of $v(t)$ and empirical parameters (e.g., Hamraoui et al., 2000; Hilpert, 2009), but all implicitly imply variable meniscus shape.

The gravitational forces G_l and G_g within the capillary are readily determined as

$$G_l = -\pi R^2 h(t)\rho_l g, \tag{6a}$$

$$G_g = -\pi R^2 [L - h(t)]\rho_g g, \tag{6b}$$

with g the gravitational acceleration.

The viscous forces F_l and F_g are determined assuming Poiseuille flow with a laminar shear stress proportional to the velocity gradient across the capillary section, thus resulting in a parabolic velocity profile in both liquid and gaseous phases. Integration of the shear rate under the Poiseuille's frame leads to

$$F_l = -8\pi\mu_l v(t)h(t), \tag{7a}$$

$$F_g = -8\pi\mu_g v(t)[L - h(t)], \tag{7b}$$

with μ_l and μ_g the liquid and gaseous dynamic viscosity, respectively.

The dissipative force W was introduced to include the effect of streamline rearrangement near the capillary entrance and its affect on the meniscus velocity. Mass conservation implies that Poiseuille flow is not valid near the entrance (where a uniform velocity profile was assumed after Sparrow et al., 1964) and that an entrance length scale $L_e = 0.06(2R)\cdot \mathrm{Re}$, with $\mathrm{Re} = v2R/\nu$ the Reynolds number, exists before the flow becomes parabolic (e.g., White, 2011). Hence, the streamlines would not be straight but would converge toward the capillary center for $h < L_e$. We hypothesize that this transition is characterized by the force W, which would dissipate kinetic energy. The corresponding head loss H_L can be taken into account using the Bernoulli's equation (Chang and Mortola, 1981). Be Section 1 the capillary entrance where the velocity profile is uniform and be Section 2 beyond L_e, where Poiseuille flow is fully developed. The head loss between the two sections can be written as

$$H_L = \frac{v_1^2}{2g}[(2\beta_2 - \alpha_2)\lambda^2 - 2\lambda\beta_1 + \alpha_1],$$

where v_1 is the average velocity in Section 1, $\lambda = 1$ is a shape factor taking into account the difference in geometry between the two sections. For a uniform velocity profile in Section 1 (i.e., at the capillary entrance), the values $\alpha_1 = 1$ and $\beta_1 = 1$ are used, while $\alpha_2 = 2$ and $\beta_2 = 4/3$ correspond to the parabolic profile at Section 2. Under these circumstances, the head loss becomes $H_L = v(t)^2/6g$, and can be used to calculate W as

$$W = -\pi R^2\rho_l g H_L = -\frac{\pi}{6}R^2\rho_l v(t)^2, \quad \text{for } v(t) \geqslant 0, \tag{8a}$$

$$W = \pi R^2\rho_g g H_L = \frac{\pi}{6}R^2\rho_g v(t)^2, \quad \text{for } v(t) < 0, \tag{8b}$$

depending on the flow direction. Near the meniscus, a similar streamline rearrangement is supposed to results in some energy loss, but it is not accounted for here as it is not known how the streamlines are affected near the moving meniscus.

Finally, the resultant ΔH of the forces at the capillary ends can be written as

$$\Delta H = \pi R^2 \Delta p, \tag{9}$$

with Δp the pressure difference at the capillary ends accounting for the hydrostatic pressure and the properties of fluid motion within the reservoirs above and below the capillary. Whereas Szekely et al. (1971) derived an expression of Δp from the energy balance that depended on the meniscus acceleration $\mathrm{d}v(t)/\mathrm{d}t$ (see Section 4), it has to be noted that an additional contribution to Δp must be included that depends on the velocity $v(t)$ when $\mathrm{d}v(t)/\mathrm{d}t = 0$. An expression that accounted for this contribution was proposed by Dreyer et al. (1994) and Xiao et al. (2006), who used a momentum balance approach and included a viscous dissipation term.

We determined Δp in Eq. (9) using a similar approach but under different assumptions. To this end, the Bernoulli's energy density flow in the liquid and gaseous reservoirs at the two capillary ends became instrumental.

The liquid reservoir was divided in two volumes, V_1 and V_2, sharing the hemispheric surface defined by the radius R. V_1 was assumed indefinitely extended, i.e., in the interval $[R, \infty)$, while V_2 was the finite volume $2/3\pi R^3$ (Fig. 2). The flow field was assumed continuous in both volumes and at their boundary, but we assumed that it was radial with velocity v in V_1 and non-radial in V_2 with uniform velocity profile. The Bernoulli energy density per unit volume at any points in the liquid reservoir was written as (e.g., Munson et al., 2006)

$$e = gz + \frac{p}{\rho} + \frac{v^2}{2},$$

where z is the position, p is the pressure and v is the velocity of an infinitesimal volume in the reservoir. Using the Gauss' divergence theorem, the rate of change of energy density within $(V_1 + V_2)$ must equal the energy density flow through the boundaries ∂V_1 and ∂V_2 of V_1 and V_2 as

$$\frac{\partial}{\partial t}\left(\int_{V_1}\rho_l e\,\mathrm{d}V + \int_{V_2}\rho_l e\,\mathrm{d}V\right) = -\int_{\partial V_1}\rho_l e\vec{v}\cdot\vec{n}\,\mathrm{d}\sigma - \int_{\partial V_2}\rho_l e\vec{v}\cdot\vec{n}\,\mathrm{d}\sigma, \tag{10}$$

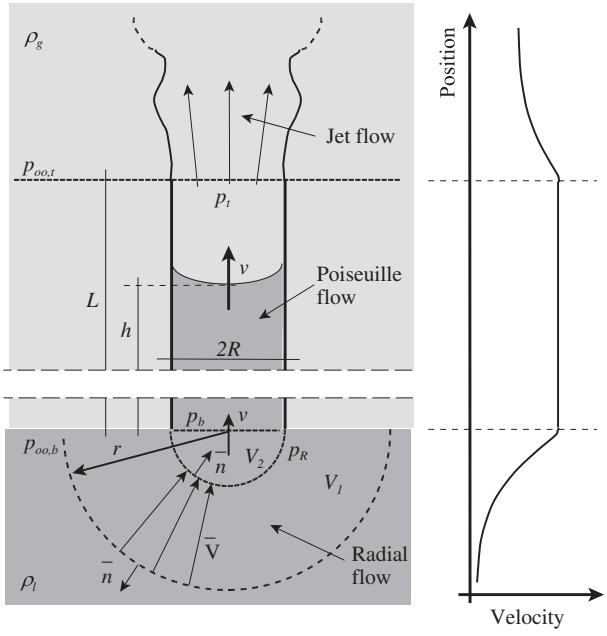

Fig. 2. Flow lines in the reservoirs above and below the capillary. Each reservoirs can be described by two domains (V_1 and V_2) characterized by radial flow (with uniform velocity profile) and non-radial flow (where the velocity profile changes from uniform to parabolic, at the capillary entrance), respectively. The flow within the capillary can be described by a laminar flow with a parabolic velocity profile, while the fluid outside the capillary and between the capillary ends is assumed to be still.

where $\vec{v}$ is the velocity vector at the boundaries ∂V_1 and ∂V_2, while $\vec{n}$ defines the normal direction at the same boundaries. To solve Eq. (10) we assumed that the phases were incompressible and that the pressure instantaneously adapted to the velocity field. We also assumed that the flow within V_1 was radial, that continuity of mass at the entrance of the capillary bottom in the volume V_2 held, and that the work exerted by gravity was negligible. Under these assumptions, the integrals in Eq. (10) resulted in

$$\begin{aligned}\frac{\partial}{\partial t}\left(\int_{V_1}\rho_l e\,\mathrm{d}V+\int_{V_2}\rho_l e\,\mathrm{d}V\right) &= \rho_l\frac{\pi}{2}R^3\frac{\mathrm{d}h}{\mathrm{d}t}\frac{\mathrm{d}^2h}{\mathrm{d}t^2}+\frac{2}{3}\rho_l\pi R^3\frac{\mathrm{d}}{\mathrm{d}t}\left(\frac{\mathrm{d}h}{\mathrm{d}t}\right)^2,\\ &\quad-\int_{\partial V_1}\rho_l e\vec{v}\cdot\vec{n}\,\mathrm{d}\sigma-\int_{\partial V_2}\rho_l e\vec{v}\cdot\vec{n}\,\mathrm{d}\sigma\\ &= \pi R^2(p_{\infty,l}-p_l)\frac{\mathrm{d}h}{\mathrm{d}t}-\frac{1}{2}\pi R^2\rho_l\left(\frac{\mathrm{d}h}{\mathrm{d}t}\right)^3,\end{aligned}$$

Combining the solutions given above for the liquid phase, and after further algebra, we obtained

$$p_l = p_{\infty,l}-\frac{1}{2}\rho_l\left(\frac{\mathrm{d}h}{\mathrm{d}t}\right)^2-\rho_l R\frac{7}{6}\frac{\mathrm{d}^2h}{\mathrm{d}t^2}, \tag{11}$$

where p_l is the pressure at the lower capillary end and $p_{\infty,l}$ is the pressure at the liquid–gas reservoir interface infinitely away from the capillary entrance. Eq. (11) shows that if the direction of motion is upward (i.e., $\mathrm{d}h/\mathrm{d}t > 0$) the pressure at the lower entrance of decreases with the square of the meniscus velocity and it decreases further if the meniscus undergoes an acceleration in the same direction (i.e., $\mathrm{d}^2h/\mathrm{d}t^2 > 0$). Under the same conditions ($\mathrm{d}h/\mathrm{d}t > 0$), the gas exits the capillary top boundary as a jet flow (Fig. 2) resulting in a pressure drop described by (Lorenceau et al., 2002)

$$p_g = p_{\infty,g}-\frac{1}{2}\rho_g\left(\frac{\mathrm{d}h}{\mathrm{d}t}\right)^2, \tag{12}$$

Combining p_l and p_g in Eqs. (11) and (12) with $p_{\infty,l} = p_{\infty,g} + \rho_g g\,L$ (i.e., the reservoirs share an interface), we obtain

$$\begin{aligned}\Delta p &= p_l - p_g =\\ &= \rho_g gL-\frac{\rho_l-\rho_g}{2}\left(\frac{\mathrm{d}h}{\mathrm{d}t}\right)^2-\frac{7}{6}\rho_l R\frac{\mathrm{d}^2h}{\mathrm{d}t^2}, \quad \text{for } \mathrm{d}h/\mathrm{d}t\geqslant 0,\end{aligned} \tag{13a}$$

$$\begin{aligned}\Delta p &= p_l - p_g =\\ &= \rho_g gL-\frac{\rho_l-\rho_g}{2}\left(\frac{\mathrm{d}h}{\mathrm{d}t}\right)^2-\frac{7}{6}\rho_g R\frac{\mathrm{d}^2h}{\mathrm{d}t^2}, \quad \text{for } \mathrm{d}h/\mathrm{d}t< 0.\end{aligned} \tag{13b}$$

Substituting the forces of Eqs. (3), (6), (7) and (8) into Eq. (2) with $h' = \mathrm{d}h(t)/\mathrm{d}t = v(t)$ and $h'' = \mathrm{d}^2h/\mathrm{d}t^2 = \mathrm{d}v(t)/\mathrm{d}t$, we obtain

$$\begin{aligned}&\frac{2}{R}\gamma\cos(\theta)-g[\rho_l h+\rho_g(L-h)]-\frac{8}{R^2}[\mu_l h+\mu_g(L-h)]h'\\ &-\frac{\rho_l}{6}h'^2+\Delta p =\\ &= [\rho_l h+\rho_g(L-h)]h'', \quad \text{for } h'\geqslant 0,\end{aligned} \tag{14a}$$

$$\begin{aligned}&\frac{2}{R}\gamma\cos(\theta)-g[\rho_l h+\rho_g(L-h)]-\frac{8}{R^2}[\mu_l h+\mu_g(L-h)]h'\\ &+\frac{\rho_g}{6}h'^2+\Delta p =\\ &= [\rho_l h+\rho_g(L-h)]h'', \quad \text{for } h'< 0,\end{aligned} \tag{14b}$$

and introducing the average density and viscosity functions $L\rho(h) = \rho_l h + \rho_g(L-h)$ and $L\mu(h) = \mu_l h + \mu_g(L-h)$ we obtain

$$\frac{2\gamma\cos(\theta)}{RL\rho(h)}-g-\frac{8\mu(h)}{R^2\rho(h)}h'-\frac{1}{6}\frac{\rho_l}{L\rho(h)}h'^2+\frac{\Delta p}{L\rho(h)}=h'' \quad \text{for } h'\geqslant 0, \tag{15a}$$

$$\frac{2\gamma\cos(\theta)}{RL\rho(h)}-g-\frac{8\mu(h)}{R^2\rho(h)}h'+\frac{1}{6}\frac{\rho_g}{L\rho(h)}h'^2+\frac{\Delta p}{L\rho(h)}=h'' \quad \text{for } h'<0, \tag{15b}$$

Finally, making Δp explicit as from Eq. (13), and after suitable algebraics, we obtain

$$\begin{aligned}\left(1+\frac{7}{6}\frac{\rho_l}{L\rho(h)}R\right)h'' &= \frac{2\gamma\cos(\theta_\infty)}{RL\rho(h)}-\frac{2A\gamma\,\mathrm{arcsinh}(Bh')}{RL\rho(h)}\\ &\quad-\frac{8\mu(h)}{R^2\rho(h)}h'-g\left(1-\frac{\rho_g}{\rho(h)}\right)-\frac{1}{2}\frac{\rho_l-\rho_g}{L\rho(h)}h'^2\\ &\quad-\frac{1}{6}\frac{\rho_l}{L\rho(h)}h'^2 \quad \text{for } h'\geqslant 0,\end{aligned} \tag{16a}$$

$$\begin{aligned}\left(1+\frac{7}{6}\frac{\rho_g}{L\rho(h)}R\right)h'' &= \frac{2\gamma\cos(\theta_\infty)}{RL\rho(h)}-\frac{2A\gamma\,\mathrm{arcsinh}(Bh')}{RL\rho(h)}-\frac{8\mu(h)}{R^2\rho(h)}h'\\ &\quad-g\left(1-\frac{\rho_g}{\rho(h)}\right)-\frac{1}{2}\frac{\rho_l-\rho_g}{L\rho(h)}h'^2\\ &\quad+\frac{1}{6}\frac{\rho_g}{L\rho(h)}h'^2 \quad \text{for } h'< 0,\end{aligned} \tag{16b}$$

which represent the governing equation of two-phase flow in capillaries. These are second-order differential equations continuous in h, h' and h'' over the entire interval $[0,L]$ and nonlinear in h and h'. For the initial conditions $h(0) = 0$ and $h'(0) = 0$ at time $t = 0$, Eq. (16a) reduces to

$$h'' = \frac{2\gamma\cos(\theta_\infty)}{RL\rho_g}\left(1+\frac{7}{6}\frac{\rho_l}{L\rho_g}R\right)^{-1}-g, \quad \text{for } h'\geqslant 0, \tag{17}$$

and demonstrates that inclusion of the rate of change of momentum of the fluids within the capillary and the rate of change of energy density outside the capillary allows us to remove the singularity in the classic Lucas–Washburn equation that implied $h''(t\to 0)\to\infty$. A similar conclusion was already achieved by Szekely et al. (1971) and Dreyer et al. (1994) but under different hypotheses.

2.2. Comparison with earlier mathematical frameworks

To demonstrate its validity, Eqs. Eqs. (16) were compared with the Lucas–Washburn equation and the approach proposed in Szekely et al. (1971).

If we apply the Lucas–Washburn assumptions in (15) ($F_g = G_g = W = 0$, Δp not explicit), neglecting inertial effects $\mathrm{d}P/\mathrm{d}t = 0$ and assuming constant contact angle ($\theta = \theta_\infty$), the terms in h'^2 and in h'' drop and Eq. (15a) becomes

$$h'' = \frac{1}{h}\left(\frac{\gamma R\cos(\theta_\infty)}{4\mu_l}+\frac{\Delta p-gh\rho_l}{8\mu_l}R^2\right), \quad \text{for } h'\geqslant 0, \tag{18}$$

which coincides with the LW equation (see Eq. (9) in Washburn, 1921).

If the assumptions used in Szekely et al. (1971) are applied to Eqs. (16) ($F_g = G_g = W = 0$, and $\theta = \theta_\infty$) but with $\mathrm{d}P/\mathrm{d}t \neq 0$ and with Δp explicit as in Eq. (13), we obtain

$$\left(h+\frac{7}{6}R\right)h''=\frac{2\gamma\cos(\theta_\infty)}{R\rho_l}-gh-\frac{8\mu_l}{R^2\rho_l}hh'-\frac{1}{2}h'^2, \quad \text{for } h'\geqslant 0, \tag{19}$$

which corresponds to Eq. (16) in Szekely et al. (1971). It is worth to note that the coefficient 7/6 on the left hand side complies with the derivation in Szekely et al. (1971) even if different hypotheses were used. However, the coefficient 1/2 in the last term differs from the one in Szekely et al. (1971) because we have not included dissipation due to the 'vena contracta' effect at the capillary entrance.

2.3. Dimensionless form

A convenient way to describe the relative contribution of each force to the meniscus dynamics described in Eqs. (16) is to derive a dimensionless expression. This can be achieved by defining the dimensionless parameters $L^* = L/h_\infty$, $\rho^* = \rho_g/\rho_l$, and $\mu^* = \mu_g/\mu_l$, and variables $t^* = t/t_c$, $h^* = h/h_\infty$, $h' = h_\infty h^{*\prime}/t_c$, and $h'' = h_\infty h^{*\prime\prime}/t_c^2$, with the characteristic time $t_c = \rho_l R^2/8\mu_l$ and equilibrium height $h_\infty = 2\gamma\cos(\theta_\infty)/\rho_l R\, g$ (i.e., Stange et al., 2003). Upon substitution of these parameters and variables, and after normalization by $2\pi R\gamma\cos\theta_\infty$, we obtain a dimensionless expression of all forces including the inertial forces I_l and I_g in Eq. (1). These are: $T^* = \cos(\theta)/\cos(\theta_\infty) = \cos^*(\theta)$, $G_l^* = -h^*, G_g^* = -\rho^*[L^* - h^*], F_l^* = -\alpha h^* h^{*\prime}, F_g^* = -\alpha\mu^*[L^* - h^*]h^{*\prime}, W^* = -\frac{1}{6}\alpha h^{*\prime 2}$ (for $h^{*\prime} \geqslant 0$), $W^* = \frac{1}{6}\alpha\rho^* h^{*\prime 2}$ (for $h^{*\prime} < 0$), $\Delta H^* = \Delta H_1^* + \Delta H_2^* + \Delta H_3^*$ with $\Delta H_1^* = \rho^* L^*, \Delta H_2^* = -\frac{1}{2}\alpha(1-\rho^*)h^{*\prime 2}, \Delta H_3^* = -\frac{7}{6}\alpha h^{*\prime\prime}$ (for $h^{*\prime} \geqslant 0$), $\Delta H_3^* = -\frac{7}{6}\alpha\rho^* h^{*\prime\prime}$ (for $h^{*\prime} < 0$), and with $I_l^* = \alpha h^* h^{*\prime\prime}$ and $I_g^* = \alpha\rho^*[L^* - h^*]h^{*\prime\prime}$. The constant α is defined as $\alpha = 4\mu_l h_\infty^2/Rt_c\cos\theta_\infty$.

The dimensionless form of Eqs. (16) can be written as

$$T^* + \sum_{l,g}(G^* + F^*) + W^* + \Delta H^* = I_l^* + I_g^*,$$

with the dimensionless forces defined above. After some rearrangements, this results in

$$\cos^*(\theta) - (1-\rho^*)h^* - \alpha(h^* + \mu^*[L^* - h^*])h^{*\prime} - \alpha\left(\frac{2}{3} - \frac{1}{2}\rho^*\right)h^{*\prime 2} = \\ = \alpha\left[h^* + \rho^*(L^* - h^*) + \frac{7}{6}\right]h^{*\prime\prime}, \quad \text{for } h^{*\prime} \geqslant 0, \tag{20a}$$

$$\cos^*(\theta) - (1-\rho^*)h^* - \alpha(h^* - \mu^*[L^* - h^*])h^{*\prime} - \alpha\left(\frac{1}{2} - \frac{2}{3}\rho^*\right)h^{*\prime 2} = \\ = \alpha\left[h^* + \rho^*(L^* - h^*) + \frac{7}{6}\rho^*\right]h^{*\prime\prime}, \quad \text{for } h^{*\prime} < 0, \tag{20b}$$

If the gas phase is excluded from Eqs. (20) (i.e., $\rho^* = \mu^* = 0$) these simplify to

$$\cos^*(\theta) - h^* - \alpha h^* h^{*\prime} - \frac{2}{3}\alpha h^{*\prime 2} = \alpha\left[h^* + \frac{7}{6}\right]h^{*\prime\prime}, \quad \text{for } h^{*\prime} \geqslant 0,$$

$$\cos^*(\theta) - h^* - \alpha h^* h^{*\prime} - \frac{1}{2}\alpha h^{*\prime 2} = \alpha h^* h^{*\prime\prime}, \quad \text{for } h^{*\prime} < 0,$$

which can be compared with earlier equations.

2.4. Model solution and parameter estimation

Eqs. (16) do not have an analytical solution. However, the second-order problem in $h'' = h''(h', h)$ were decomposed into a system of two first-order ordinary differential equations of the form $\{y = h', y' = y'(y, h)\}$, which were next integrated numerically with an explicit finite difference technique.

Three type of tests were carried out using Eqs. (16); Test 1 did not include the gaseous phase (i.e., $\rho_g = \mu_g = 0$) and variable contact angle (i.e., $A = B = 0$); Test 2 included both liquid and gaseous phases, but did not include variable contact angle ($A = B = 0$); Test 3 included both phases and also variable contact angle, i.e., Eqs. (16) were used in their complete form. Finally, Test 4 was performed using the complete Eqs. (16) as Test 3 to highlight the effect of parameter uncertainty on model accuracy.

Model validation was performed against experiments in Test 1 and Test 2 by solving the direct problem, while Test 3 and Test 4 required some parameter estimation. This was carried out by solving the inverse problem according to the Levenberg–Marquardt algorithm (e.g., Doerthy, 2004). Validations and parameter estimations are presented in graphical and tabular forms. Model accuracy was assessed *via* the correlation coefficient (R) and normalized root mean square error (NRMSE) against experiments as

$$R = \frac{\mathrm{cov}(m,o)}{\sigma_m\sigma_o}, \quad \mathrm{NRMSE} = \frac{\sqrt{\frac{1}{n}\sum_{i=1}^{n}(m_i - o_i)^2}}{\max\{o_i\} - \min\{o_i\}},$$

with m and o the modeled and observation points, respectively.

3. Results

Water, dodecane, diethyl ether, ethanol, and silicon (all displacing standard air) were tested with Eqs. (16) for a range of capillary radii and gravitational accelerations. In each instance, the full and simplified forms of Eqs. (16) were compared with the original LW equation, and previous models.

3.1. Water and air

Experiments using water in a glass capillary (redrawn from Hamraoui et al., 2000) were used to test Eqs. (16). We also considered the original LW equation, and the modified LW equation proposed in Hamraoui et al. (2000) here referenced as HTNY2000, which included a parameterized source of dissipation equivalent to dynamic contact angle localized near the meniscus.

The results in Fig. 3a show that LW and Eqs. (16) of Test 1 and Test 2 returned similar R (94–96%) and NRMSE (14–16%), thus

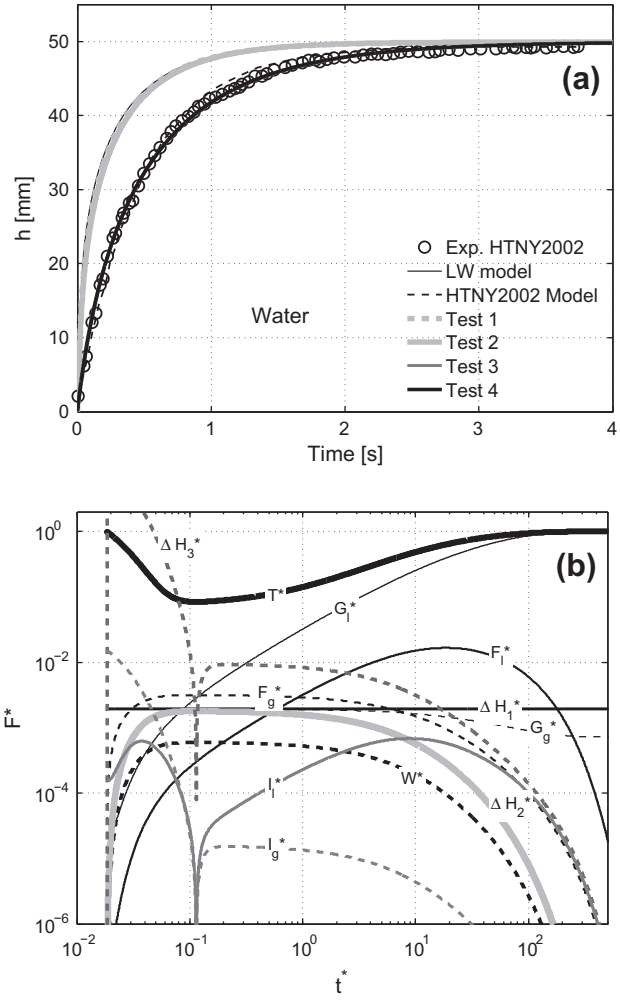

Fig. 3. (a) Experimental and modeled rise of water and air in a glass capillary. Experimental data are redrawn from Hamraoui et al. (2000). (b) Dimensionless forces corresponding to Test 4 of panel (a).

Table 1
Parameters used to model water–air rise in a glass capillary from Hamraoui and Nylander (2002). Values in parenthesis were estimated. L and G stay for liquid and gas phases, respectively. C and V stay for constant and variable contact angle, respectively.

Water–air		LW	HTNY2000 [a]	Eq. (16)			
				Test 1	Test 2	Test 3	Test 4
dP/dt		=0	$\neq 0$[b]	$\neq 0$	$\neq 0$	$\neq 0$	$\neq 0$
Phase		L	L	L	L, G	L, G	L, G
Reservoir effect		–	–	√	√	√	√
Contact angle		C	V	C	C	V	V
R	(mm)	0.295	0.295	0.295	0.295	0.295	0.295
γ	(mN m^{-1})	72	72	72	72	72	(71.9)
θ_∞	(°)	0	0	0	0	0	0
ρ_l	(kg m^{-3})	998	998	998	998	998	(997.7)
ρ_g	(kg m^{-3})	–	0	0	1.2	1.2	(1.2)
μ_l	(mPa s)	1	1	1	1	1	(0.99)
μ_g	(mPa s)	–	0.0186	0	0.0186	0.0186	(0.0186)
L	(m)	–	–	–	0.08[b]	0.08[b]	0.08[b]
A	(–)	–	–	0	0	(52.34)	(51.94)
B	(s m^{-1})	–	–	0	0	(0.265)	(0.261)
R %		94.97	99.87	95.44	95.67	99.91	99.92
NRMSE %		15.91	2.08	14.98	14.26	1.1	0.98

[a] The HTNY2000 model made use of an additional calibration parameter not reported here.
[b] $L = 0.08$ m was assumed.

meaning that including the gas phase in Test 2 improved only slightly the NRMSE as compared to Test 1. Using Eqs. (16) as in Test 3 substantially improved the water–air rise and resulted in $R > 99.9\%$ and NRMSE = 1.1%. The HTNY2000 model did not account for the gas phase but included variable contact angle using one additional fitting parameters (not reported in Table 1, HTNY2000), thus being intermediate between Eqs. (16) of Test 2 and Test 3. Test 4 was carried out with the aim of highlighting uncertainties in density, viscosity, and surface tension such as, for instance, due to temperature. This test showed that very small variations of these parameters (<0.1%), could improve R to 99.92% and NRMSE to 0.98% (Test 4, Table 1). This improvement was minor in the case of water–air rise, but we will show that uncertainties in the physical parameters of other fluids could largely affect model accuracy. We also note that Eqs. (16) of Test 3 and Test 4, resulted in the lowest NRMSE and highest R as compared to any other models tested here (Table 1).

Fig. 3b depicts each dimensionless force driving the meniscus dynamics. The gas inertia I_g^* and retardation effects in the gaseous and liquid reservoirs ΔH_2^* and ΔH_3^*, respectively, were the most important forces after the tension T^* at the onset of flow. Soon after, F_l^*, F_g^* and W^* effects became highly relevant when the velocity reached the maximum value. Near equilibrium, only G_l^* equilibrated T^*. It has to be noted that W^* played a role as important as inertial and friction. The cuspids in $\Delta H_3^*, I_g^*$ and I_l^* were due to a change in sign for h''.

3.2. Dodecane and air

A comparison was performed between Eqs. (16) and the experiments of dodecane (n-dodecane, $C_{12}H_{26}$, 99% purity) and air in a glass capillary (redrawn from Zhmud et al., 2000). The LW equation and the ZTH2000 model were used for comparison.

The LW equation and Eqs. (16) of Test 1 show that neglecting the gas phase produced the largest deviation from the experiments (NRMSE > 11.63%). Test 2, which included the gas phase, and Test 3, which used the full Eqs. (16), achieved an accurate description of dodecane–air flow ($R = 99.96$ % and NRMSE in the range 3.88–5.54%). The ZTH2000 model achieved $R = 99.78\%$ and NRMSE = 2.91% (Table 2, Fig. 4a) even if it did not include the gas phase. However, it included an additional dissipative force proportional to the product qhh'^2 for h' larger than a critical velocity that was interpreted as a turbulence dissipation term. Regardless of the mathematical structure of this term (discussed in detail in Section 4), the dimensional parameters q and critical velocity for turbulence (not reported in Table 2) were fitted to experimental data, thus making it parametrically equivalent to Eqs. (16) of Test 3, which required calibration of A and B.

The effect of the gas phase in the dodecane–air system was more important than in the water–air system. This is evidenced by a NRMSE decreasing only marginally from 14.98% (Test 1) to 14.26% mm (Test 2) in the water–air system as compared to a decrease from 11.63% (Test 1) to 5.54% mm (Test 2) in the dodecane–air system.

Variable contact angle introduced in Test 3 contributed substantially to improve model accuracy in both water and dodecane systems. Finally, Test 4 shows that accounting for uncertainty in the density (<0.4%), viscosity (<10%) and surface tension (<13%) reduced the error to NRMSE = 1.65% (Table 2). As compared to all other models, Eqs. (16) in Test 4 returned the highest R and smallest NRMSE against experiments.

The dimensionless forces in Fig. 4b show again that T^*, I_l^*, I_g^* and ΔH^* were important at the onset of flow. However, at intermediate times, F_l^* and F_g^* appeared to be the most important forces, whereas $\Delta H^*, I_l^*, I_g^*$, and W^* had second order effects. It has to be noted that W^* was an important terms in the dodecane–air system as in the water–air system.

3.3. Diethyl ether and air

We have tested Eqs. (16) on diethyl ether ($(C_2H_5)_2O$, 99% purity) displacing air in a glass capillary (redrawn from Zhmud et al., 2000). For this test we have also considered the LW equation and the ZTH2000 model already introduced for the dodecane–air system, which included here an additional friction force due to the gas phase. This experiment was particularly interesting to validate

Table 2
Parameters used to model dodecane–air rise in a glass capillary from Zhmud et al. (2000). Values in parenthesis were estimated. L and G stay for liquid and gas phases, respectively. C and V stay for constant and variable contact angle, respectively.

Dodecane–air		LW	ZTH2000 [a]	Eq. (16)			
				Test 1	Test 2	Test 3	Test 4
dP/dt		=0	=0	$\neq 0$	$\neq 0$	$\neq 0$	$\neq 0$
Phase		L	L	L	L, G	L, G	L, G
Reservoir effect		–	–	√	√	√	√
Contact angle		C	C	C	C	V	V
R	(mm)	0.1	0.1	0.1	0.1	0.1	0.1
γ	(mN m^{-1})	25	25	25	25	25	(28.48)
θ_∞	(°)	17	17	17	17	17	17
ρ_l	(kg m^{-3})	750	750	750	750	750	(746.7)
ρ_g	(kg m^{-3})	–	–	0	1.2	1.2	(1.20)
μ_l	(mPa s)	15	15	15	15	15	(13.49)
μ_g	(mPa s)	–	–	0	0.0186	0.0186	(0.0186)
L	(m)	–	–	–	0.1[b]	0.1[b]	0.1[b]
A	(–)	–	–	0	0	(191.59)	(339.78)
B	(s m^{-1})	–	–	0	0	(0.0207)	(0.0367)
(mm)	65	65	65	65	65	73.1	
R %		99.97	99.78	99.97	99.96	99.96	99.92
NRMSE %		12.01	2.91	11.63	5.54	3.88	1.65

[a] The model ZTH2000 made use of two additional fitting (empirical) parameters not reported here.
[b] $L = 0.1$ m was assumed.

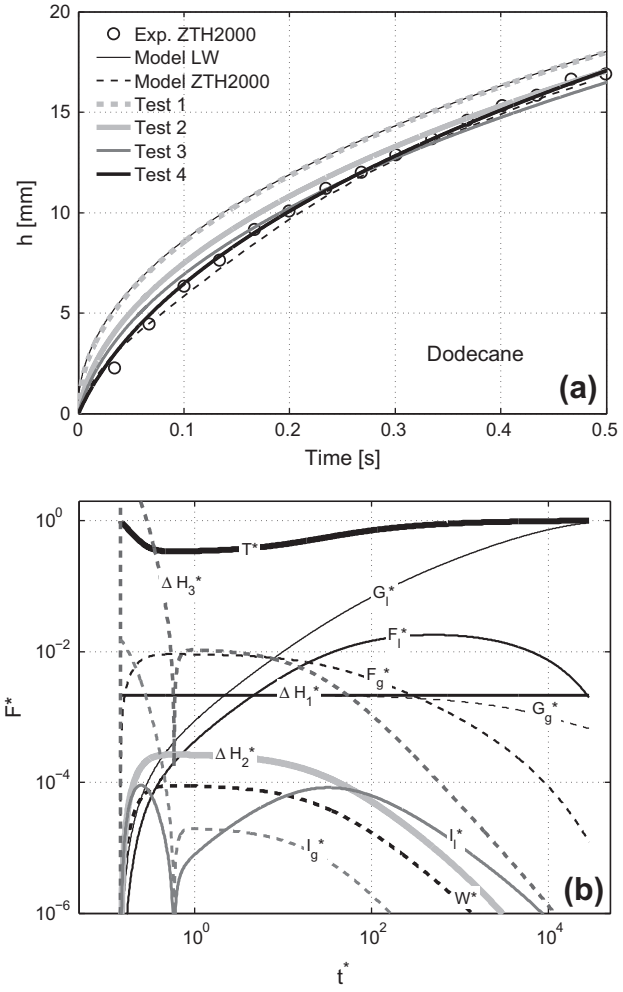

Fig. 4. (a) Experimental and modeled rise of dodecane and air in a glass capillary. Experimental data are redrawn from Zhmud et al. (2000). (b) Dimensionless forces corresponding to Test 4 of panel (a).

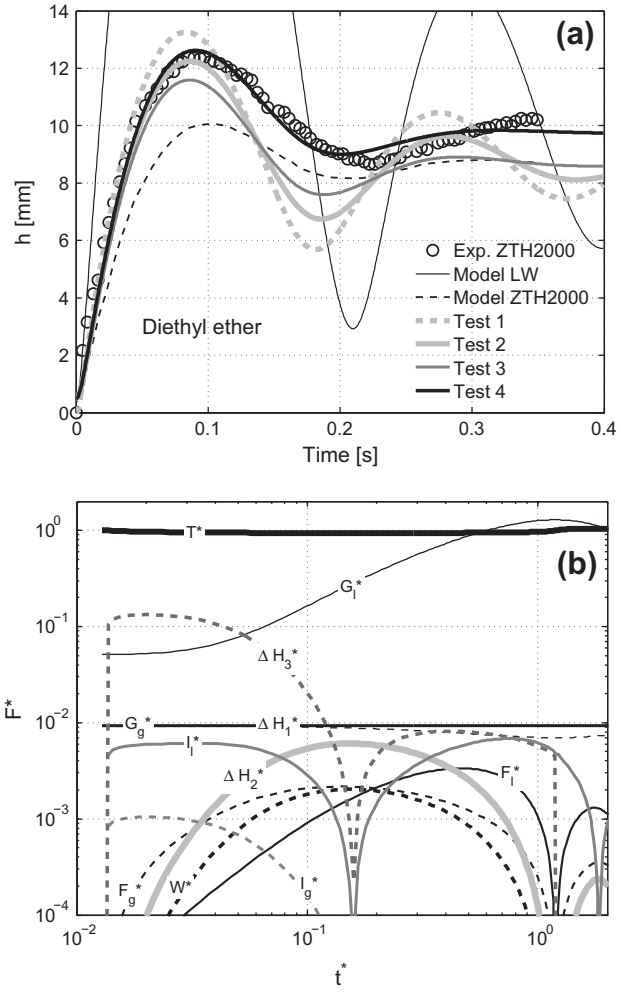

Fig. 5. (a) Experimental and modeled rise of diethyl ether and air in a glass capillary. Experimental data are redrawn from Zhmud et al. (2000). (b) Dimensionless forces corresponding to Test 4 of panel (a).

our and previous models because the specific fluid properties and capillary geometry resulted in large oscillations[1] around the equilibrium height h_∞ (Fig. 5).

The LW equation largely departed from the experimental observations (NRMSE = 73.55%) and resulted in a relatively low correlation (R = 72%). Test 1, which was used with the parameters provided in Zhmud et al. (2000) and did not account for the gas phase, significantly improved the prediction of $h(t)$ and resulted in R = 82.92% and NRMSE = 13.57% against the experiment (Table 3). Introducing the gas phase in Eqs. (16) of Test 2, resulted in R = 92.32% and NRMSE = 10.33%, which was further improved by variable contact angle in Test 3 (R = 97.12% and NRMSE = 9.48%). The ZTH2000 model included the gas friction F_g, yet neglecting all other gas-phase contributions to the meniscus dynamics, and resulted in R = 94.98% and NRMSE = 12.76% (Table 3).

Analogously to the experiment with dodecane (Fig. 4a), the ZTH2000 model also considered a parameterized turbulence-induced dissipation term, which required estimation of two parameters not reported in Table 3. This feature made the ZTH2000 model parametrically similar to Eqs. (16) of Test 3, which required estimation of A and B. However, Eqs. (16) of Test 3 resulted in better accuracy and suggested that the reservoirs retardation effects, variable contact angle and the gas phase significantly contributed to the meniscus dynamics within the capillary. We also note from the NRMSE of Test 1 (13.57%), Test 2 (10.33%), Test 3 (9.48%) and the ZTH2000 model that the gas phase had a relatively important effect as compared to variable contact angle.

Test 4 was performed by fitting the physical parameters in Eqs. (16), and resulted in R = 98.90% and NRMSE = 2.98% by adjustments not exceeding 5% change (Table 3). Overall, Test 4 resulted in the highest R and smallest NRMSE as compared to all other tests and models (Table 3) and could visibly capture the meniscus dynamics over time (Fig. 5a).

Fig. 5b shows that $\Delta H^*, I^*_{l,g}$ and as well as W^*, and $F^*_{l,g}$ were secondary as compared to the T^* and G^*_l. However, because the model achieved a high accuracy against experiments, we infer that the oscillations observed in panel (a) strongly depended on the interplay between all these forces and resulted in the observed fading oscillations over time.

3.4. Ethanol and air

In this test we have used Eqs. (16) to describe ethanol–air rise in a glass capillary (redrawn from Hamraoui et al., 2000). We also considered the LW and HTNY2000 models already used for water–air rise.

[1] Eq. (16) always results in oscillatory solutions because it is a nonlinear second-order differential equation. Depending on the circumstances, these oscillations may not be detected by the sensitivity of experimental apparata.

Table 3
Parameters used to model diethyl ether–air rise in a glass capillary from Zhmud et al. (2000). Values in parenthesis were estimated. L and G stay for liquid and gas phases, respectively. C and V stay for constant and variable contact angle, respectively.

Diethyl ether–air		LW	ZTH2000[a]	Eq. (16)			
				Test 1	Test 2	Test 3	Test 4
dP/dt		=0	=0	≠0	≠0	≠0	≠ 0
Phase		L	L, G[b]	L	L, G	L, G	L, G
Reservoir effect		–	–	√	√	√	√
Contact angle		C	C	C	C	V	V
R	(mm)	0.5	0.5	0.5	0.5	0.5	0.5
γ	(mN m^{-1})	16.7	16.7	16.7	16.7	16.7	(18.29)
θ_∞	(°)	26	26	26	26	26	26
ρ_l	(kg m^{-3})	710	710	710	710	710	(691.2)
ρ_g	(kg m^{-3})	–	–	0	1.2	1.2	(1.18)
μ_l	(mPa s)	22	22	22	22	22	(23.14)
μ_g	(mPa s)	–	0.0186	0	0.0186	0.0186	(0.0185)
L	(m)	–	0.05	–	0.05	0.05	0.05
A	(–)	–	–	0	0	(0.0321)	(0.0447)
B	(s m^{-1})	–	–	0	0	(128.87)	(115.27)
R %		72.01	94.98	82.92	92.32	97.12	98.90
NRMSE %		73.55	12.76	13.57	10.33	9.48	2.98

[a] The model ZTH2000 made use of two additional fitting (empirical) parameters not reported here.
[b] The effect of the gas phase was included only in the viscous friction contribution F_g.

Table 4
Parameters used to model ethanol–air rise in a glass capillary from Hamraoui et al. (2000). Values in parenthesis were estimated. L and G stay for liquid and gas phases, respectively. C and V stay for constant and variable contact angle, respectively.

Ethanol–air		LW	HNTY2000 [a]	Eq. (16)			
				Test 1	Test 2	Test 3	Test 4
dP/dt		=0	≠0	≠0	≠0	≠ 0	≠0
Phase		L	L	L	L, G	L, G	L, G
Reservoir effect		–	–	√	√	√	√
Contact angle		C	V	C	C	V	V
R	(mm)	0.295	0.295	0.295	0.295	0.295	0.295
γ	(mN m^{-1})	22	22	22	22	22	(22.21)
θ_∞	(°)	0	0	0	0	0	0
ρ_l	(kg m^{-3})	789	789	789	789	789	(805.01)
ρ_g	(kg m^{-3})	–	–	–	1.2	1.2	(1.19)
μ_l	(mPa s)	11.7	11.7	11.7	11.7	11.7	(11.3)
μ_g	(mPa s)	–	–	–	0.0186	0.0186	(0.0173)
L	(m)	–	–	–	0.08[b]	0.08 [b]	0.08 [b]
A	(–)	–	–	0	0	(0.0053)	(0.0094)
B	(s m^{-1})	–	–	0	0	(238,383)	(2862)
R %		99.23	97.98	99.45	99.28	99.32	99.36
NRMSE %		3.56	4.01	2.96	2.83	2.44	2.38

[a] The model HTNY2000 made use of an additional fitting (empirical) parameter not reported here and includes an inertial term referred to as the reservoir effect whereas it corresponds to inertial effects within the capillary.
[b] L = 0.08 m was assumed.

The accuracy of all models and tests in Table 4 was very high (R ranged within 97.98–99.36%, and NRMSE ranged within 2.38–4%), with Eqs. (16) performing marginally better (Fig. 6a). Inclusion of the gas phase and variable contact angle improved only slightly the accuracy of Eqs. (16) *versus* gas phase-only. As already observed before, accounting for uncertainty in the density, viscosity and surface tension (<6%) produced the highest R and lowest NRMSE (Table 4).

The dimensionless forces in Fig. 6b highlight that F^*_{lg}, ΔH^*, and W^* had a small impact as compared to G^*_l. The type of behaviors in Fig. 6b resembles the transitions highlighted in Stange et al. (2003) for silicon fluid, where three regions of flow could neatly be distinguished.

3.5. Silicon and air in microgravity

In this final test, Eqs. (16) were used to describe silicon fluid displacing air in a Plexiglass capillary (redrawn from Stange et al., 2003). This experiment was particularly interesting because was performed in microgravity conditions ($g \simeq 0.02$ m s^{-2} was used here), hence for very small G_l and G_g. The LW and SDR2003 models were used for comparison.

The results in Fig. 7 show that the LW equation largely departed from the experiments (NRMSE > 100%, Table 5), while the SDR2003 model reached an accuracy of R = 99.99% and NRMSE = 1.19%. Use of Eqs. (16) of Test 1 and Test 2 did not achieve such accuracy, whereas introducing the gas phase and variable contact angle in Test 3 led to R = 99.74% and NRMSE = 3.26% (Table 5). We note here that the SDR2003 model included two empirical parameters from Jiang et al. (1979) which were obtained by fitting in Hoffman Hoffman (1975) to describe variable contact angle, thus being equivalent to Eqs. (16) of Test 3. Similarly to all previous experiments, Test 4 was run by fine-tuning all physical parameters (<0.9%) to assess parameter uncertainty, and led to the best model-to-experiment fit (R = 99.98% and NRMSE = 0.55%).

In microgravity ($g \simeq 0.02$ ms^{-1}), G^*_g and G^*_l did not disappear fully and contributed to the meniscus movement along the capillary together with the tension T^*. Viscous friction (F^*_g and F^*_l), dissipation at the entrance (W^*), as well as the reservoir retardation

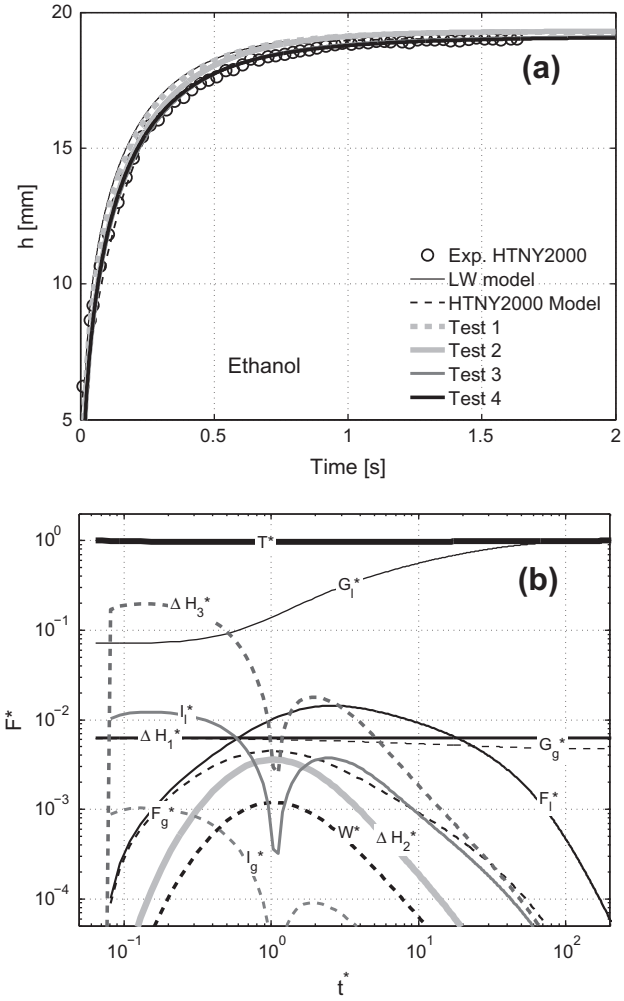

Fig. 6. (a) Experimental and modeled rise of ethanol and air in a glass capillary. Experimental data are redrawn from Hamraoui et al. (2000). (b) Dimensionless forces corresponding to Test 4 of panel (a).

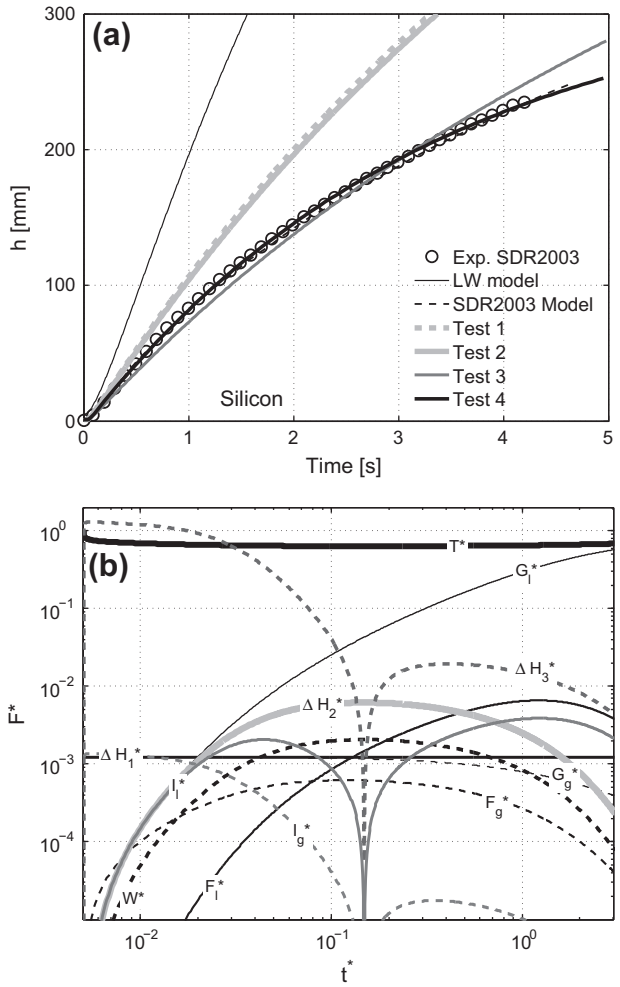

Fig. 7. (a) Experimental and modeled rise of silicon fluid and air in a Plexiglas capillary under microgravity conditions ($g = 10^{-4}$ m s^{-2} was assumed here). Experimental data are redrawn from Stange et al. (2003). (b) Dimensionless forces corresponding to Test 4 of panel (a).

(ΔH_1^* and ΔH_2^*) had only minor effects, while ΔH_3^* was important at the onset of flow.

3.6. Summary of experimental results

Table 6 summarizes the best values R and NRMSE obtained in all tests presented here. In general, the LW equation was largely improved by all other models (Table 6). However, under the same parametrical degrees of freedom (i.e., two fitting parameters), Eqs. (16), Test 3, returned higher accuracy in capturing experimental observations as compared to HTNY2000, ZTH2000 and SDR2003 models. Uncertainties in physical parameters accounted for in Eqs. (16), Test 4, may be considered as additional degrees of freedom and resulted in further improvements of R and NRMSE.

Overall, Eqs. (16) proved to be robust to describe multiphase capillary flows in various conditions including different liquids, capillary radii, and gravitational accelerations.

3.7. Reynolds number and flow conditions

We have analyzed the flow rate in all experiments presented above with the scope to highlight transitions to turbulently flows. For this analysis, the Reynolds number Re_g and Re_l relative to the gas and liquid phases, respectively, were calculated using Eqs. (16) of Tests 4. Fig. 8 shows that the flow rates were always below the threshold for turbulence (Re < 2300), and suggests that a distributed source of turbulence dissipation was not justified in Zhmud et al. (2000).

Table 5
Parameters used to model silicon–air rise in a Plexiglas capillary in microgravity ($g \simeq 0.02$ ms^{-2}) from Stange et al. (2003). Values in parenthesis were estimated. L and G stay for liquid and gas phases, respectively. C and V stay for constant and variable contact angle, respectively.

Silicon–air		LW	SDR2003 [a]	Eq. (16)			
				Test 1	Test 2	Test 3	Test 4
dP/dt		=0	≠0	≠0	≠0	≠0	≠0
Phase		L	L	L	L, G	L, G	L, G
Reservoir effect		–	√	√	√	√	√
Contact angle		C	V	C	C	V	V
R	(mm)	4	4	4	4	4	4
γ	(mN m^{-1})	16.9	16.9	16.9	16.9	16.9	(17.33)
θ_∞	(°)	0	0	0	0	0	0
ρ_l	(kg m^{-3})	818	818	818	818	818	(817.61)
ρ_g	(kg m^{-3})	–	–	–	1.2	1.2	(1.19)
μ_l	(mPa s)	0.818	0.818	0.818	0.818	0.818	(0.825)
μ_g	(mPa s)	–	–	–	0.0186	0.0186	(0.0186)
L	(m)	–	–	–	0.4 [b]	0.4 [b]	0.4 [b]
A	(–)	–	–	0	0	(0.0751)	(0.0696)
B	(s m^{-1})	–	–	0	0	(49,224,839)	(996,123)
R %		99.93	99.99	99.77	99.75	99.74	99.98
NRMSE %		103.5	1.19	29.71	28.15	3.21	0.55

[a] The model SDR2003 made use of two additional fitting (empirical) parameters to describe variable contact angle (see Eq. (5) in Stange et al., 2003).
[b] $L = 0.4$ m was assumed.

Table 6
Summary of quantitative estimators of accuracy against experiments of two-phase capillary rise for the Lucas–Washburn equation (LW), the HTNY2000 model (Hamraoui et al., 2000), the ZTH2000 model (Zhmud et al., 2000) and the SDR2003 model (Stange et al., 2003) aggregated in column "Other models", and Eq. (16). L and G stay for liquid and gas phases, respectively.

	LW	Other models	Eq. (16), Test 3	Eq. (16), Test 4
Phases	L	L, G[a]	L, G	L, G
Fitted parameters	0	2–3	2	2–7
R %	72.01–99.97	94.98–99.99	97.12–99.96	98.84–99.98
NRMSE %	3.56–103.5	1.19–12.76	1.1–9.48	0.55–2.98

[a] The ZTH2000 model partly included the effect of the gas phase while all other models only accounted for the liquid phase.

3.8. Analysis of molecular and thermodynamic parameters

It is meaningful to interpret the parameters A and B within the Eyring theory of rate processes (Blake and Haynes, 1969; Eyring (1935)) and assess the molecular and thermodynamic parameters at the solid–liquid–gas interface defined by

$$n = \frac{A\gamma}{2k_B T_K}, \tag{21}$$

$$\lambda = n^{-1/2}, \tag{22}$$

$$K^0 = \frac{1}{2B\lambda}, \tag{23}$$

with $k_B = 1.38 \times 10^{-23}$ J/K the Boltzmann constant and $T_K = 293$ K (20 °C) the assumed temperature. The values of n, λ and K^0 were calculated *a posteriori* from A and B of Tests 4. It is important to note here that only indicative values are available for some substances.

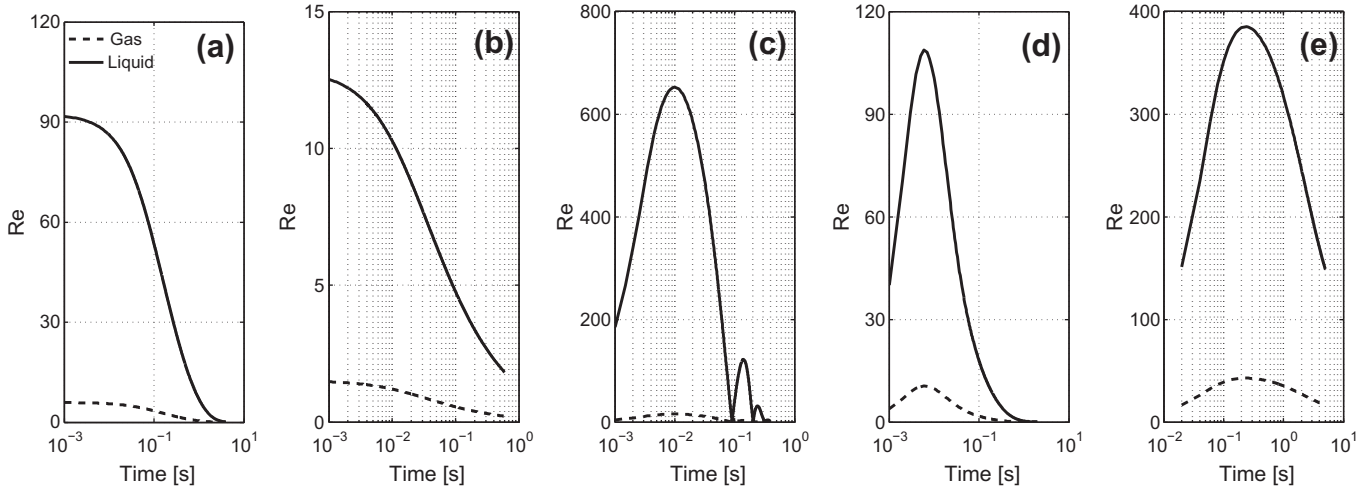

Fig. 8. Reynolds number calculated *a posteriori* for the gas and liquid phases in the two-phase systems with air and (a) water, (b) dodecane, (c) diethyl ether–air, (d) ethanol, and (e) silicon.

For example, $n \approx 5.2 \times 10^{13}$ cm^{-2} for benzene displacing water, and $n \approx 2 \times 10^{13}$ cm^{-2} for water displacing benzene, with $\lambda \approx n^{-1/2} \approx 1$ Å,[2] and $K^0 \approx 5 \times 10^2$ s^{-1} (Blake and Haynes, 1969).

Table 7 shows two interesting aspects. The number of activated sites n per unit area changed over about five orders of magnitude, and implied a strong dependency on the substances interacting at the capillary wall. The calculated distance between activated sites λ, ranged within 0.29–0.62 Å. These values are particularly meaningful because they are expected to be in the order of magnitude of the molecule size, hence around the Å. The Eyring rate constant K^0, i.e., the frequency at which activated solid sites adsorb activated liquid sites per unit time, must be a large number if expressed in seconds. Clearly, when a liquid displaces a gas as in the experiments analyzes here, K^0 is expected to be particularly large. Our calculations show K^0 values ranging within 10^2–10^{10} s^{-1} (Table 7).

Table 7
Molecular (n and λ) and thermodynamic (K^0) parameters calculated *a posteriori* using Eqs. (21)–(23) for multiphase flows in which various liquids displace air in capillaries.

Liquid		Water	Dodecane	Diethyl ether	Ethanol	Silicon
A[a]	(–)	51.94	339.78	0.0447	0.0095	0.0696
B[a]	(s m^{-1})	0.26	0.037	115.28	2862.1	996,120
n	(10^{16} m^{-2})	46,223	119,630	10.124	2.5967	14.702
λ	(10^{-10} m)	0.465	0.28912	0.3143	0.6206	0.2608
K^0	(10^5 s^{-1})	412,360	4,708,000	13.801	0.28151	0.01925

[a] Values calculated by calibration. The reference temperature is assumed to be T_K = 293.15 K (20 °C).

4. Discussion

We have presented a mathematical framework to describe multiphase flows in capillary tubes which accounts for conservative and non-conservative forces in both liquid and gaseous phases within the capillary and in the adjacent reservoirs at the capillary ends. In deriving Eqs. (16) for multiphase capillary flows we have taken into account various aspects that improve the description of the meniscus dynamics. The original contributions presented in this work are discussed.

Dissipative forces (i.e., W_l and W_g) have been introduced to describe the energy dissipation involved in the adjustment of the velocity profile from uniform to parabolic within an entrance length in both liquid and gaseous phases. Other sources of energy dissipation can be included such as due to the *vena contracta* and the streamline rearrangement near the meniscus. Levine et al. (1980) proposed that dissipation at the meniscus that could be described by viscous forces extended over a length scale equivalent to the meniscus height (form the contact line to the depression) and to an additional length scale linked to surface irregularities. The two contributions were described by a function of the meniscus shape (sphere sector) and by a function of the capillary radius, slip coefficient, and contact angle, respectively (see Eq. 3.14 Levine et al., 1980). Regardless of the explicit formalisms proposed here and in Levine et al. (1980), the two approaches converge to identify a localized source of energy dissipation that causes a reduction of the meniscus velocity within the capillary that scales with h'^2 (here) and with h and h' in Levine et al. (1980).

Aspects of energy dissipation localized at the meniscus have been also considered from a different perspective. For example, Hamraoui et al. (2000) have argued whether a variable contact angle can be interpreted as a dissipative process involving a friction coefficient. In their work, Hamraoui et al. (2000) have introduced a term proportional to the meniscus velocity $\beta h'$ to describe the rate of change of the contact angle, where β is an empirical dimensional parameter. This approach replaces the hyperbolic function of Bh' used in Eq. (5) (Blake and Haynes, 1969), but does not introduce an alternative explanation to variable contact angle. It is to be noted that the hyperbolic function in Blake and Haynes (1969) was derived on first principles and, from a theoretical view point, the coefficients therein used were only related to the thermodynamical and molecular properties of the substances under investigation, and to the rate of displacement of liquid molecules over a surface (see Eq. (5)). The rate of displacement K^0 can be linked, by matter of fact, to a frictional parameter (Blake and Haynes, 1969) as also recalled later by Hamraoui et al. (2000). Other formulations exist to describe variable contact angle by means of linear and exponential functions (e.g., Joos et al., 1989; Ralston et al., 2008). However, a careful inspection suggests that those formulations converge to the hyperbolic model proposed in Blake and Haynes (1969) as this can show either a linear regime (for $(\gamma/n)(\cos\theta - \cos\theta_\infty) \ll k_B T_K$) or an exponential regime ($(\gamma/n)(\cos\theta - \cos\theta_\infty) \gg k_B T_K$). Because the

[2] Note the power scaling $\lambda \approx n^{-1/2}$ with respect to the original formulation. The negative exponent must be used for congruity between the dimensions of A and B.

Blake and Haynes (1969) approach is general, we have not considered alternative descriptions of variable contact angle within the framework proposed here.

Another important aspect that we have developed in this work is related to the effect of the reservoirs at the capillary ends. The approach presented here is inspired by the work presented in Szekely et al. (1971), which develops around the Newton's Law in the form $F \times v\mathrm{d}t = \mathrm{d}E_k$, with E_k the kinetic energy. By writing $F \times v\mathrm{d}t = \mathrm{d}E_k$ with $F = \pi R^2 \Delta p$ and Δp a pressure deficit, and solving the rate of change of the kinetic energy for Δp within an infinite reservoir, Szekely et al. (1971) obtained the pressure at the lower capillary end as a function of the meniscus acceleration h''. However, for consistency with the Bernoulli principle, the pressure at the lower capillary end should also be determined by the meniscus velocity h'. Using a similar approach Dreyer et al. (1994) could overcome this inconsistency, showing that the pressure at the capillary ends is affected by three terms proportional to h', h'' and h'^2, respectively. We have used an approach that differs from the ones mentioned above and that makes use of the Bernoulli energy density. By integrating the time change of Bernoulli energy density within the space domain at the two capillary ends (Fig. 2), we could describe the pressure at the capillary inlet and outlet as a function of the meniscus velocity h'^2 and acceleration h'', but neglecting the term in h' found in Dreyer et al. (1994, 2006). As already demonstrated in Szekely et al. (1971) and Dreyer et al. (1994), accounting for the effect of reservoir removes the singularity point in the Lucas–Washburn equation and allows for a numerical integration of capillary dynamics over any non-negative values of the initial capillary height $h(0)$. Also in this case, it is interesting to note how different working hypotheses have led to similar results. For example, our approach shows that the integrated Bernoulli energy density flow results in a term proportional to $7/6h''$, which coincides with Eq. (15) in Szekely et al. (1971).

The framework presented in this paper did not include a dissipative term proportional to qhh' responsible for turbulent drag as proposed in Zhmud et al. (2000). The assumed laminar flow conditions do not preclude the presence of turbulence as long as this is strictly localized at the entrance of the capillary and for high Reynolds number regimes (Brittin, 1945). However, the term proposed by Zhmud et al. (2000) does not fully satisfy these conditions; in fact, it appears to be proportional to the capillary height h, thus suggesting that turbulent drag would occur along the entire liquid body in the capillary. Regardless of the presence or absence of turbulence in capillary flows, introduction of this non-conservative term implies the introduction of a first-and second-order discontinuity in the equation describing the meniscus velocity (i.e., turbulent drag exists only for $v > v_c$, with v_c a critical velocity), and the use of two dimensional fitting parameter (q and v_c) that cannot be directly measured. The Reynolds numbers derived using Eqs. (16) do not show transitions to turbulent flows in any experiments analyzed here. However, we believe that one of the most challenging aspects to improve capillary dynamics is the understanding of the circumstances under which localized turbulent flow regimes can develop and how this might affect the meniscus movement. In this respect, Zhmud et al. (2000) work can be considered as an initial framework to develop further for circumstances of tested high Reynolds numbers.

An aspect that requires careful attention is the treatment of compressible phases. The equation presented here considers incompressible phases under the assumption that the capillary ends are open and in contact with infinitely extended reservoirs at rest. In these circumstances, compressibility may be neglected in solving the equation of motion of the meniscus. However, we recognize that compressible phases should be considered in close-end capillaries.

More generally, use of the mathematical framework proposed here with existing experimental data supports two important observations.

The first is that the dynamics of multiphase flows in capillaries are substantially more complex than how it is conceived within the classic Lucas–Washburn framework. The LW equation, which can best capture the meniscus dynamics near equilibrium, fails to describe the initial movement. A number of contributions to the Lucas–Washburn equations have been successful in improving the dynamics of liquids of relatively high density and viscosity. For example, the models described in Hamraoui et al. (2000) and Zhmud et al. (2000) were relatively accurate for the dynamics of water and ethanol, while for low density fluids such as diethyl ether, the overall modeled dynamics were characterized by large differences as compared to the experimental observations. The improvements introduced in the mathematical framework presented here (Eqs. (16)) show that discrepancies with experimental observations can be overcome for a larger range of system characteristics when the system is explicitly described by multiple phases. Tests presented in Section 3 show that Eqs. (16) largely increased the correlation with observations of the capillary height over time while sensibly decreasing the normalized root mean square error.

The second important aspect is that our mathematical framework and tests demonstrate that uncertainties in the values of the physical parameters can largely affect the accuracy in describing capillary dynamics. For example, relatively small variations in the fluid and gaseous density and viscosity in all Tests 4 led to a remarkable increase in correlation coefficient and decrease in error against experiments. These uncertainties can be ascribed to various causes, the temperature effect on fluid density, viscosity and surface tension being most likely over others.

Finally, additional aspects should be addressed in future studies of multiphase flows in capillaries including chemically heterogenous phases (e.g., mixtures of fluids) and thermodynamic effects of the mass exchange between liquid and gaseous phases at the meniscus (e.g., the effect of temperature and vapor pressure).

5. Conclusions

A mathematical description of multiphase flows in capillaries was proposed. The second-order nonlinear differential equation explicitly described the non-stationary meniscus progression within a capillary under the action of conservative forces (gravity and interfacial tensions), non-conservative forces (viscous friction along the capillary and energy dissipation near the inlet), and under the retardation effect of the fluids in the reservoirs at the capillary ends. This multiphase flow equation was applied in a wide range of two-phase systems (water, dodecane, diethyl ether, ethanol, silicon and air), capillary dimensions (0.1–4 mm), and gravitational accelerations (terrestrial and microgravity). The results shows a significant improvement of the correlation R (97.5–99.96%) and error NRMSE (0.55–9.52%) against earlier single-phase models based on the Lucas–Washburn equation (R in the range 72–99.99% and NRMSE in the range 1.19–>100%). Based on our results, we support the hypothesis that an explicit accounting of multiple phases, the gaseous phase in particular, is crucial to accurately predict flows in capillaries.

Acknowledgments

F. Alonso-Marroquin was supported by the Australian Postdoctoral Fellowship, Australian Research Council, Discovery Project DP0772409. The authors thank Dr. David Fletcher for the important discussion on processes near the meniscus and the two anonymous

reviewers, who have addressed us to several important aspects of capillary processes and improvements to the content presented here.

References

Bell, J.M., Cameron, F.K., 1906. The flow of liquids through capillary spaces. J. Phys. Chem. 10, 658–674.

Bico, J., Quere, D.J., 2001. Rise of liquids and bubbles in angular capillary tubes. Colloid Interface Sci. 247, 162–166.

Blake, T.D., Haynes, J.M., 1969. Kinetics of liquid/liquid displacement. J. Colloid Interface Sci. 30, 421–423.

Brittin, W.E., 1945. Liquid rise in a capillary tube. J. Appl. Phys. 17, 37–44.

Chang, H.K., Mortola, J.P., 1981. Fluid dynamic factors in tracheal pressure measurement. J. Appl. Physiol. 51, 218–225.

Cox, R.G., 1998. Inertial and viscous effects on dynamic contact angles. J. Fluid Mech. 357, 249–278.

Dreyer, M., Delgado, A., Rath, H.-J., 1994. Capillary rise of liquids between parallel plates under microgravity. J. Colloid Interface Sci. 163, 158–168.

Doerthy, J., 2004. PEST Model-Independent Parameter Estimation, fifth ed., p. 336.

Eyring, H., 1935. The activated complex and the absolute rate of chemical reactions. Chem. Rev. 17, 65–77.

Eyring, H., 1935. The activated complex in chemical reactions. J. Chem. Phys. 3, 107–115.

De Gennes, P.G., 1985. Wetting: statics and dynamics. Rev. Modern Phys. 57, 827–863.

Hamraoui, A., Thuresson, K., Nylander, T., Yaminsky, V., 2000. Can a dynamic contact angle be understood in terms of a friction coefficient? J. Colloid Interface Sci. 226, 199–204.

Hamraoui, A., Nylander, T., 2002. Analytical approach for the Lucas–Washburn equation. J. Colloid Interface Sci. 250, 415–421.

Hilpert, M., 2009. Effects of dynamic contact angle on liquid infiltration into horizontal capillary tubes: (semi)-analytical solutions. J. Colloid Interface Sci. 337, 131–137.

Hoffman, R.L., 1975. A study of the advancing interface. I. Interface shape in liquidgas systems. J. Colloid Interface Sci. 50, 228–241.

Jiang, T.-S., Oh, S.-G., Slattery, J.C., 1979. Correlation for dynamic contact angle. J. Colloid Interface Sci. 69, 74–77.

Joos, P., van Remoortere, P., Bracke, M.J., 1989. The kinetics of wetting in a capillary. Colloid Interface Sci. 136, 136–189.

Levine, S., Lowndes, J., Watson, E.J., Neale, G., 1980. A theory of capillary rise of a liquid in a vertical cylindrical tube and in a parallel-plate channel: Washburn equation modified to account for the meniscus with slippage at the contact line. J. Colloid Interface Sci. 73, 136–151.

Lorenceau, E., Quéré, D., Ollitrault, J.-Y., Clanet, C., 2002. Gravitational oscillations of a liquid column in a pipe. Phys. Fluids 14, 1985–1992.

Lucas, R., 1918. Uber das Zeitgesetz des kapillarenAufstiegs von Flussigkeiten. Kolloid Zeitschr. 23, 15 (in German).

Maggi, F., Pallud, C., 2010. Space agriculture in micro-and hypo-gravity: a comparative study of soil hydraulics and biogeochemistry in a cropping unit on earth, mars, the moon and the space station. Planet. Space Sci. 58, 1996–2007. doi:10.1016/j.pss.2010.09.025.

Martic, G., Gentner, F., Seveno, D., Coulon, D., De Coninck, J., Blake, T.D., 2002. A molecular dynamics simulation of capillary imbibition. Langmuir 18, 7971–7976.

Munson, B.R., Young, D.F., Okiishi, T.H., 2006. Fundamentals of Fluid Mechanics, fifth ed. John Wiley & Sons, Inc.

Popescu, M., Ralston, J., Sedev, R., 2008. Capillary rise with velocity-dependent dynamic contact angle. Langmuir 24, 12710–12716.

Ralston, J., Popescu, M., Sedev, R., 2008. Dynamics of wetting from an experimental point of view. Annu. Rev. Mater. Res. 38, 23–43.

Sparrow, E.M., Lin, S.H., Lundgren, T.S., 1964. Flow development in the hydrodynamic entrance region of tubes and ducts. Phys. Fluids 7, 338–347.

Stange, M., Dreyer, M.E., Rath, A.J., 2003. Capillary driven flow in circular cylindrical tubes. Phys. Fluids 15, 258.

Szekely, J., Neumann, A.W., Chuang, Y.K., 1971. The rate of capillary penetration and the applicability of the Washburn equation. J. Colloid Interface Sci. 35, 273.

Washburn, E.W., 1921. The dynamics of capillary flow. Phys. Rev. 17, 273–283.

White, F.M., 2011. Fluid Mechanics, seventh ed. McGraw Hill, p. 862.

Zhmud, B.V., Tiberg, F., Hallstensson, K., 2000. Dynamics of capillary rise. J. Colloid Interface Sci. 228, 263–269.

Xiao, Y., Yang, F., Pitchumani, R., 2006. A generalized analysis of capillary flows in channels. J. Colloid Interface Sci. 298, 880–888.